COBEM 2021 26th International Congress of Mechanical Engineering
November 22-26, 2021, Virtual Congress, Brazil
ABCM Associação Brasileira de Engenharia e Ciências Mecânicas

VARYING GEOMETRY OF MICRO-CHANNEL FLOW SIMULATED WITH LATTICE BOLTZMANN METHOD

Arthur do Canto Pivetta
Cirilo Seppi Bresolin
Universidade Federal do Rio Grande do Sul, Rua Sarmento Leite, 425
cirilo.bresolin@ufrgs.br

Abstract. *Microchannel heat exchangers have gained importance with the development of technology that requires heat exchange in small scale, such as electronics. The lattice Boltzmann method presents good capacity to simulate complex geometry and small-scale physics. This paper presents a comparison between different geometries of microchannels with varying spacing between internal obstacles and different boundary conditions, using the lattice Boltzmann method to simulate with varying Reynolds numbers. Observed output parameters were: Nusselt number, average temperature and Darcy friction factor. The results present an increased Nusselt number and Darcy friction factor for smaller spacing between obstacles. Nusselt number presents varying behavior with variation of Reynolds for the different boundary conditions, especially for small Reynolds numbers (around 1). Average temperature increases by decreasing Reynolds number or spacing between objects, as expected.*

Keywords: *lattice Boltzmann method, LBM, micro-channel, heat transfer enhancement.*

1. INTRODUCTION

In the last years, as the technology evolved, many applications for heat transfer in micro-scale have presented themselves, be it in the electronics industry, micro-structures construction technology, or in the medical engineering field, among others. (Ghadirzadeh and Kalteh, 2017)

A good example of a device that deals with heat transfer is micro-scale is the microchannel heat exchanger. Borquist *et al.* (2016) exemplifies microchannels applications as ranging from electronics cooling to harnessing waste energy, commenting on how it uses fluid-filled channels with reduced scales which produce effective heat and mass transfer.

The lattice Boltzmann method (LBM) is a numerical method for the simulation of many physical phenomena. Its use has been increasing in recent years, as has been verified by Mesa (2014) in his master's thesis.

This method is based on the resolution of Boltzmann's transport equation and on the kinetic theory of gases. It is remarked that the LBM has advanced in the last few decades, becoming a successful method for simulating complex physical, chemical and fluid mechanics problems, also presenting the ability to process complicated boundary geometries easily with acceptable accuracy. It is important to say that one of the reasons it is useful is that this method is able to simulate situations in which the continuity assumption is no longer valid such as when the scale of the problem is too small. (Jahanshaloo *et al.*, 2016)

This paper will use simulation with the lattice Boltzmann method to analyse the heat exchange and the friction factor for a micro-channel with obstacles of varying spacing.

To evaluate validity of the method, a comparison is made between the analytical result of a parallel flow and the simulation results. The chosen problem to compare is that of parallel flow between parallel plates, as presented by Schlichting (1979), since it is a simpler version of the situations analysed in this paper.

2. METHODOLOGY

In this paper both the fluid flow and the thermal field are solved using the lattice Boltzmann method (LBM). The LBM solves numerically the Boltzmann transport equation. For that, a set of discrete microvelocities e_i (Fig. 1) and its probability discrete function f_i are defined.

The evolution equation for the density distribution function f_i is:

$$f_i(\vec{x} + \delta_t \vec{e}_i, t + \delta_t) - f_i(\vec{x}, t) = -\frac{1}{\tau}[f_i(\vec{x}, t) - f_i^{(eq)}(\vec{x}, t)] \quad i = 0, 1, ...8 \tag{1}$$

where x is the position in lattice length units (l.l.), δ_t is the time step (in lattice time units, l.t.), e_i is the microvelocity i, defined by Eqs. 2, t is time (in l.t.), τ is the relaxation time, which controls the approach to equilibrium and is defined by Eq. 3, $f_i^{(eq)}$ is the equilibrium distribution function defined by Eq. 4. It is important to note that the LBM uses dimensionless units (referred to as lattice length, lattice time, lattice velocity, etc.).

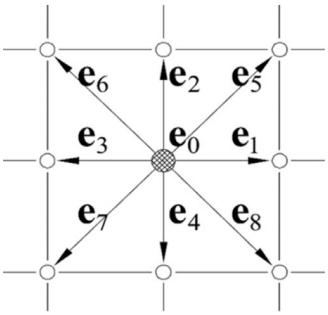

Figure 1. Microvelocities of a site for the lattice Boltzmann method.

The microvelocities are defined as:

$$\vec{e_i} = [cos(\pi(i-1)/2, sen(\pi(i-1)/2] \qquad i = 1,2,3,4 \tag{2a}$$

$$\vec{e_i} = [\sqrt{2}(cos(\pi(i-4-\frac{1}{2})/2, sen(\pi(i-4-\frac{1}{2})/2] \qquad i = 5,6,7,8 \tag{2b}$$

$$\vec{e_0} = [0] \qquad i = 0 \tag{2c}$$

where i is the position seen on Fig. 1.

The Chapman-Enskog expansion of Eq.1 results in the following relation between the relaxation time and kinematic viscosity:

$$\tau = 3\nu + \frac{1}{2} \tag{3}$$

where ν is the kinematic viscosity of the fluid in analysis.

The equilibrium distribution function $f_i^{(eq)}$, which is the result of the discretization of the Maxwell-Boltzmann distribution, is defined as:

$$f_i^{(eq)} = t_i\rho[1 + 3(\vec{e_i}\cdot\vec{u}) + \frac{9}{2}(\vec{e_i}\cdot\vec{u})^2 - \frac{3}{2}\vec{u}\cdot\vec{u}], \quad t_0 = \frac{4}{9}, \quad t_i = \frac{1}{9}, i = 1:4; \quad t_i = \frac{1}{36}, i = 5:8. \tag{4}$$

where t_i is the weight of the i position in the lattice, ρ is the density and u is the velocity and defined as follows:

$$\sum_{n=0}^{8} f_i = \rho \quad \sum_{n=1}^{8} f_i\vec{e_i} = \rho\vec{u} \tag{5}$$

The boundary conditions utilized are: periodic boundary condition for the eastern and western boundaries, which treats the channel as a section of an infinitely repeating pattern; walls (with the no-slip condition) in the northern and southern border. These boundary conditions are formulated as described by Zou and He (1996).

The pressure gradient is the flow driving force, imposed in this simulation by body force, which is set as an input parameter.

The lattice Boltzmann method that was utilized for analysis of the thermal field is analogous to the method for analysis of fluid flow. The analogous function to the density distribution function f_i is the energy distribution function g_i. The evolution function g_i is defined by the lattice Boltzmann method as:

$$g_i(\vec{x} + \delta_t\vec{e_i}, t + \delta_t) - g_i(\vec{x}, t) = -\frac{1}{\tau_g}[g_i(\vec{x}, t) - g_i^{(eq)}(\vec{x}, t)] \quad i = 0, 1, ...8 \tag{6}$$

where most of the variables has already been defined after being presented on Eq. 1. The variables that have not been defined yet are analogous to the ones on Eq. 1 and are as follows: g_i is the value of the energy distribution function in the $\vec{e_i}$ direction, τ_g is the relaxation time defined by Eq. 7, $g_i^{(eq)}$ is the equilibrium distribution function defined by Eq. 8.

The relaxation time τ_g is defined as

$$\tau_g = 3\alpha + \frac{1}{2} \tag{7}$$

where α is the thermal conductivity. The equilibrium distribution function $g_i^{(eq)}$ is defined as:

$$g_i^{(eq)} = t_i T[1 + 3(\vec{e}_i \cdot \vec{u}) + \frac{9}{2}(\vec{e}_i \cdot \vec{u})^2 - \frac{3}{2}\vec{u} \cdot \vec{u}], \quad t_0 = \frac{4}{9}, \quad t_i = \frac{1}{9}, i = 1:4; \quad t_i = \frac{1}{36}, i = 5:8. \tag{8}$$

where most of the variables has already been defined after being presented on Eq. 4, and the only variable not yet defined is T, temperature, which is defined as:

$$\sum_{n=0}^{8} g_i = T \tag{9}$$

Of note, but not yet mentioned, the heat flux for each of the sites in the lattice:

$$\vec{q} = \vec{u}T + \sum_{n=1}^{8} g_i \vec{e}_i \tag{10a}$$

$$\tag{10b}$$

The Reynolds number is calculated as shown by Eq. 11:

$$Re = \frac{u_m Ly}{\nu} \tag{11}$$

where u_m is the average velocity through the channel in lattice velocity units (l.l./l.t.), Ly is the total channel height, and ν is the fluid kinematic viscosity.

The Darcy friction factor (f_{Darcy}) is calculated as shown by Eq. 12:

$$f_{Darcy} = 2\left(\frac{dp}{dx}\right)\frac{Ly}{u_m^2} \tag{12}$$

Newton's cooling law defines:

$$q = h_x A(T_x - T_{bulk}) \tag{13}$$

where q is the heat exchange, A is the area that is exchanging heat, h_x is the convection heat transfer coefficient at position x (defined by Eq. 15, T_x is the wall temperature at position x, and T_{bulk} is the bulk temperature at position x, defined as:

$$T_{bulk} = \frac{\int_0^{Ly} \rho u c_p T dy}{\int_0^{Ly} \rho u c_p dy} \tag{14}$$

where c_p is the specific heat of the fluid.

The convection heat transfer coefficient at position x is defined as:

$$h_x = \frac{-k \left.\frac{dT}{dy}\right|_{y=0}}{T_x - T_{bulk}} \tag{15}$$

where k is the thermal conductivity.

The local heat transfer coefficient, h_x, can be used to calculate the local Nusselt number through Eq. 16:

$$Nu_x = \frac{h_x Ly}{k} \tag{16}$$

which in turn can be used to calculate the average Nusselt number of a section:

$$Nu = \frac{1}{b-a}\int_a^b Nu_x dx \tag{17}$$

where a and b are, respectively, the starting and ending positions of the section.

3. PROBLEM DESCRIPTION

The problem consists of a variation on the problem of parallel flow through a straight channel as described by Schlichting (1979). Schlichting describes this problem as being a steady flow between two parallel flat walls. The variations on this problem are: there is heating in the south wall and the heated wall has obstacles on the flow side.

Two different south wall thermal boundary conditions were used: a prescribed and constant temperature and a prescribed and constant heat flux. Different simulations were made each with the following Reynolds numbers: 1, 5, 10, 25, 50 and 100. The obstacles that are present on the south wall are square-shaped. For each case, different spacing lengths between obstacles were simulated as can be observed in Figs. 2 to 4.

The size of the channel in the simulation is 2400 lattice length units in the x direction and 240 lattice length units in the y direction. The obstacles have a height and width of 60 lattice length units. Figs. 2 to 4 present three of the cases with variation of the spacing length between the objects. The spacing length in these figures is of 60, 120 and 180 lattice length units, which, respectively, receive the label of L1, L2 and L3 when used in legend. The average Nusselt number is calculated from the start of the last obstacle to the spacing length after the object (i.e. for the L1 spacing, the Nusselt number is calculated from the start of the last object to 60 lattice length units after the obstacle).

Figure 2. Wall with spacing length between objects of 60 lattice length units, labeled L1.

Figure 3. Wall with spacing length between objects of 120 lattice length units, labeled L2.

Figure 4. Wall with spacing length between objects of 180 lattice length units, labeled L3.

For all cases the entrance has a constant temperature and fully developed fluid flow. The northern wall is adiabatic and has a no-slip boundary condition. The southern wall has either a prescribed temperature or a constant heat flux, while also having a no-slip boundary condition for both cases. The entrance and exit present a periodic boundary condition for the fluid flow, which means that the exit and entrance have exactly the same fluid flow (this represents and infinitely repeating channel). The outflow thermal boundary is a convective boundary condition as described by Lou *et al.* (2013).

4. RESULTS AND DISCUSSION

This section presents the validation made with the use of a similar (but simpler) problem that has an analytical solution, the grid convergence analysis and the results and discussion for the channels of the various geometries.

4.1 Validation with parallel plates

As commented previously, this paper analyses a variation on the parallel flow through a straight channel as described by Schlichting (1979). Thus, a comparison of results between the analytical result of this problem and the simulated result with LBM. Fig. 5 presents this comparison for the velocity profile, where u_x is the velocity in the x direction, u_∞ is the mean velocity, ny is the number of elements in the y direction used in the simulation.

For 9 elements or more in the vertical direction, the results overlap with the analytical curve to such a degree that it is indistinguishable in Fig. 5, validating the method to a reasonable degree.

4.2 Grid Convergence

To check grid convergence a series of simulations of heated plates with no obstacles with different number of elements was evaluated comparing the Nusselt number and other parameters with the number of elements. Fig. 6 presents the Nusselt number comparison, which is representative of the overall behavior observed.

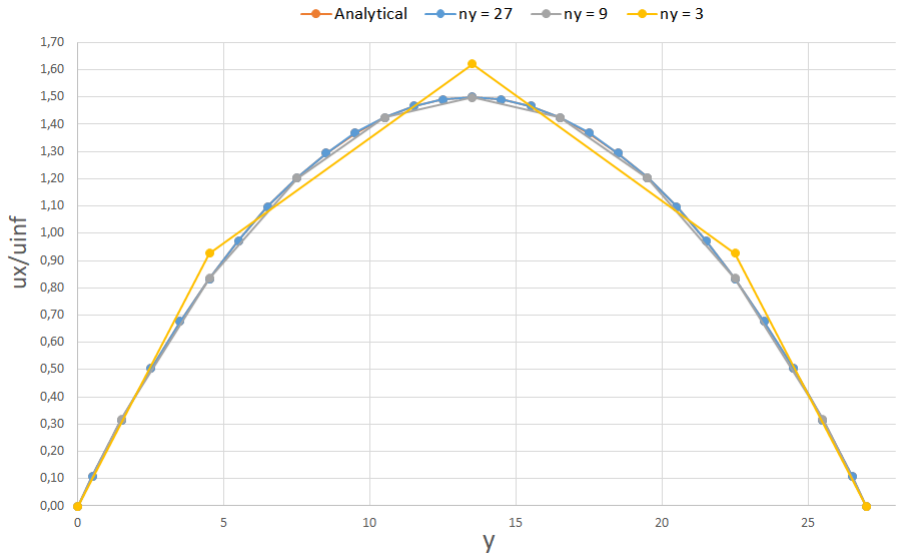

Figure 5. Comparison between analytical and simulated results.

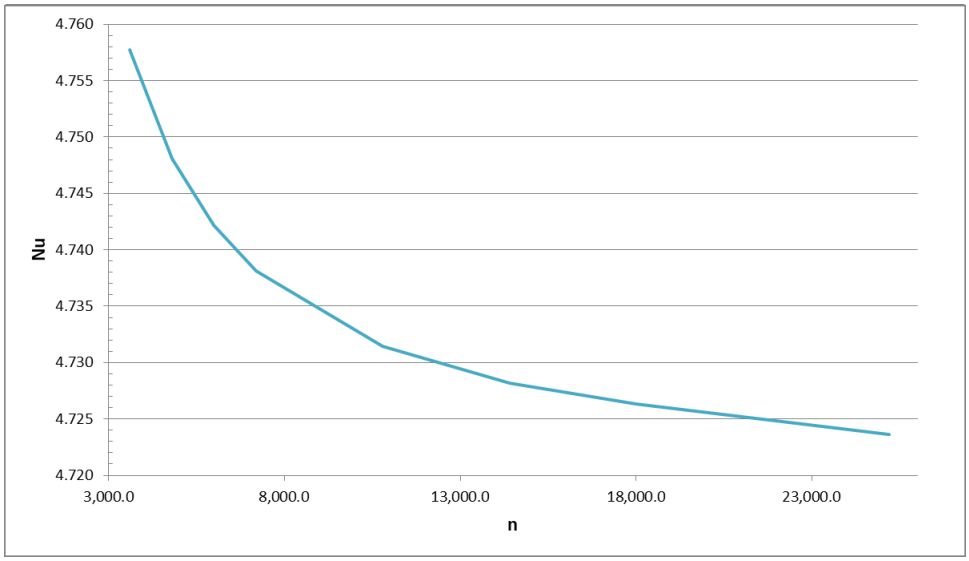

Figure 6. Nusselt number by number of elements.

Fig. 6 presents the desired behavior when seeking grid convergence, which is a decrease in the slope with the increase of the number of elements. Moreover, the difference in the Nusselt number for each of these situations is small to begin with.

4.3 Results for varied geometries

Given that the simulation is of a forced flow, temperature is unable to affect significantly the velocities, thus the velocities are considered independent from the different temperature boundaries, and only dependent on the single input parameter of body force, which will result in a different Reynolds number. For that reason, velocity results for both temperature boundaries are presented as one.

Fig. 7 present the Darcy friction factor for different Reynolds numbers and different geometries. Since the scale is too large to show the smaller variation that occur for higher Reynolds numbers, a different scale is also presented in the same figure. Fig. 8 presents the product of the Darcy friction factor and Reynolds number for different Reynolds numbers and different geometries.

As expected, when the Reynolds number increases, the friction factor decreases. Also as expected, an increase in the spacing between obstacles (which results in a smaller number of obstacles) results in a smaller friction factor.

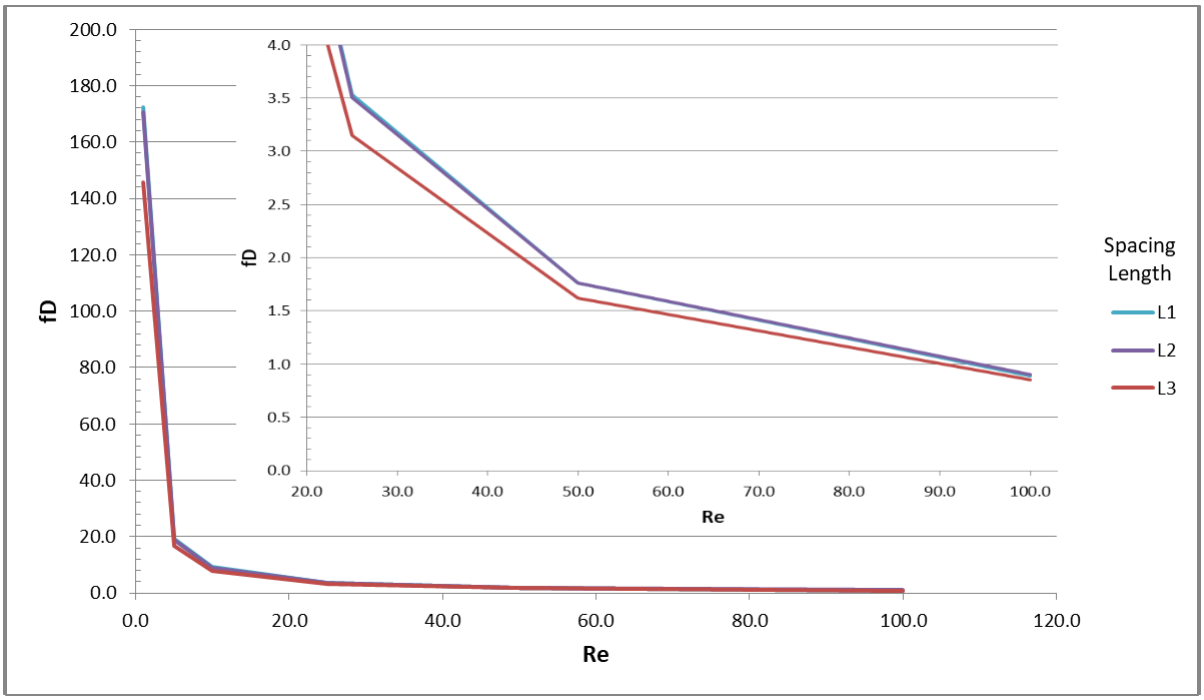

Figure 7. Darcy friction factor for different Reynolds numbers and different spacing lengths. In this figure, L1, L2 and L3 are, respectively, 60, 120 and 180 units of lattice length of space between objects.

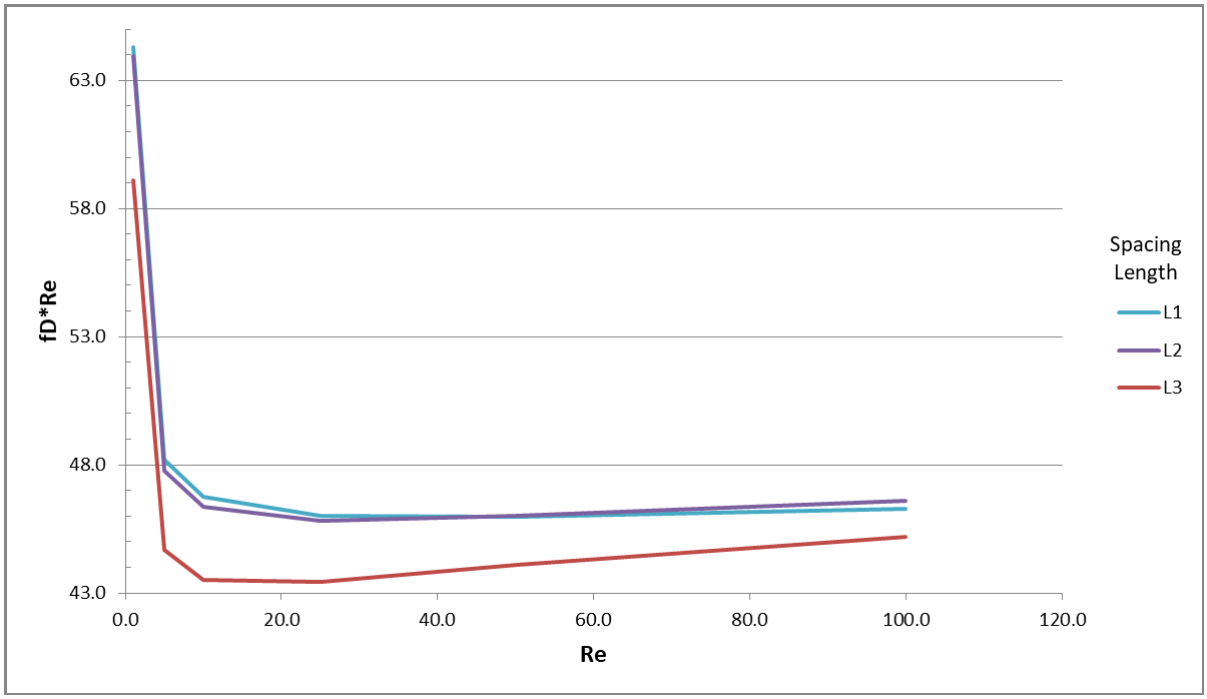

Figure 8. Product of the Darcy friction factor and Reynolds number for different Reynolds numbers and different spacing lengths. In this figure, L1, L2 and L3 are, respectively, 60, 120 and 180 units of lattice length of space between objects.

4.3.1 Prescribed Temperature

Figs. 9 and 10 present the results for the simulation with prescribed temperature in the south boundary. Fig. 9 presents the Nusselt number for different Reynolds numbers and different spacing lengths. Fig. 10 presents the average temperature for different Reynolds numbers and different spacing lengths.

For the Nusselt number, as expected, the smaller spacing length between objects presents higher values, while an increase in this spacing produces smaller Nusselt numbers. Of note here is that for small Reynolds numbers (around 1) an increase of the Reynolds number produces a decrease in the Nusselt number, up to a Re of 10 to 20, where an increase

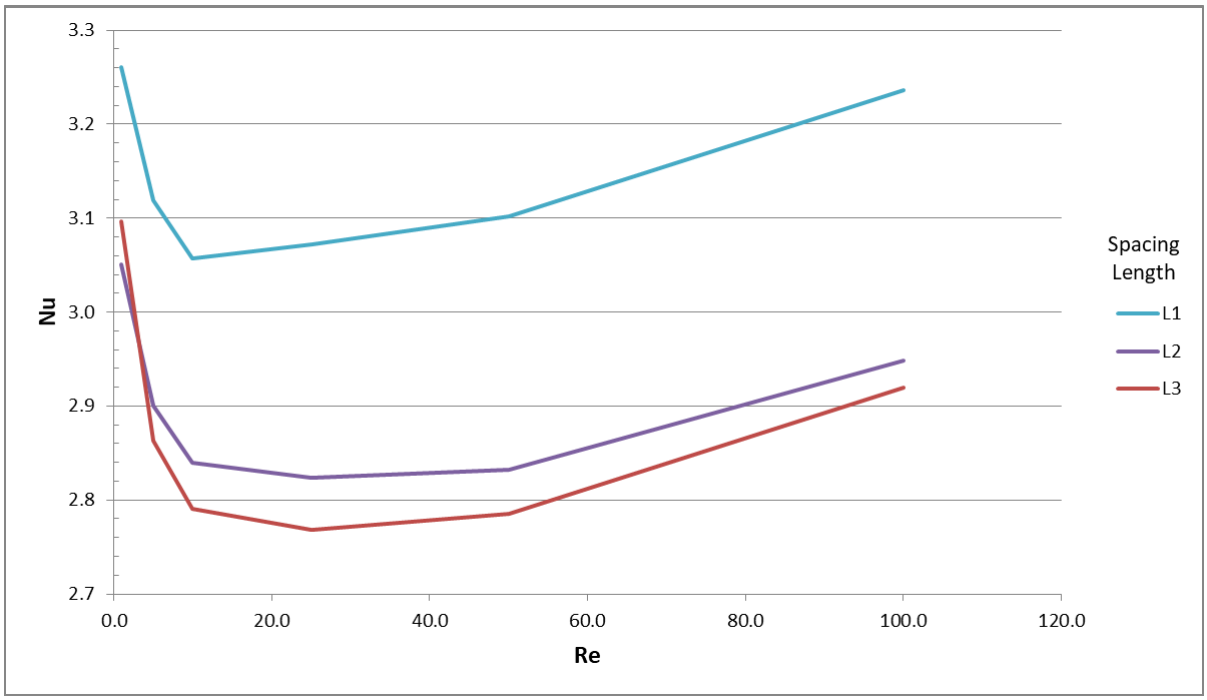

Figure 9. Nusselt by Reynolds for different spacing lengths for the prescribed temperature boundary. In this figure, L1, L2 and L3 are, respectively, 60, 120 and 180 units of lattice length of space between objects.

in the Reynolds number will result in an increase in the Nusselt number, which is the expected behavior.

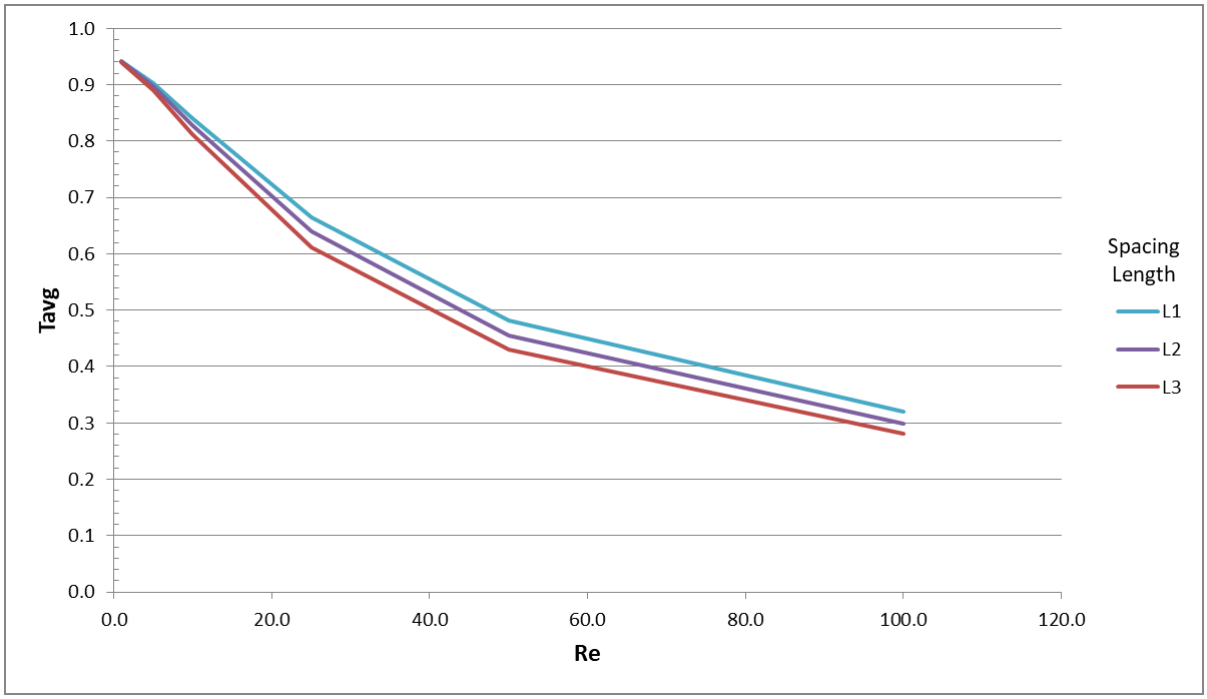

Figure 10. Temperature by Reynolds for different spacing lengths for the prescribed temperature boundary condition. In this figure, L1, L2 and L3 are, respectively, 60, 120 and 180 units of lattice length of space between objects.

For the temperatures the behavior is only as expected: for low Reynolds numbers the average temperature tends to the temperature of the prescribed temperature on the wall, varying very little with spacing between obstacles. As the Reynolds number increases, the average temperature decreases and it is noticeable that for the smaller spacing lengths a higher average temperature is achieved, which is in line with the higher Nusselt numbers observed in Fig. 9.

4.3.2 Constant Heat Flux

Figs. 11 and 12 present the results for the simulation with constant heat flux in the south boundary. Fig. 11 presents the Nusselt number for different Reynolds numbers and different spacing lengths. Fig. 12 presents the average temperature for different Reynolds numbers and different spacing lengths.

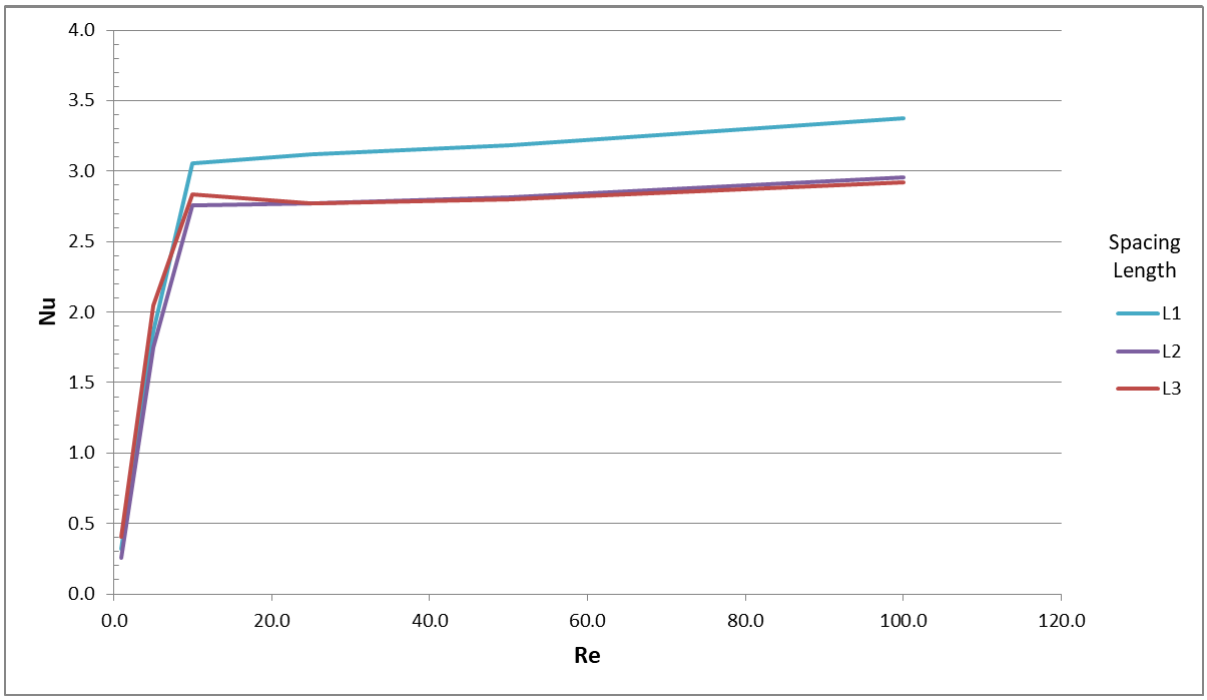

Figure 11. Nusselt by Reynolds for different spacing lengths for the constant heat flux boundary condition. In this figure, L1, L2 and L3 are, respectively, 60, 120 and 180 units of lattice length of space between objects.

It can be observed that up to a Reynolds number of around 10, the Nusselt number increases at a steep ratio with no remarkable differences between the different spacings. However, for higher values of Reynolds number, the Nusselt number increases in a smaller ratio and it is noticeable that the smallest spacing presents a higher Nusselt number.

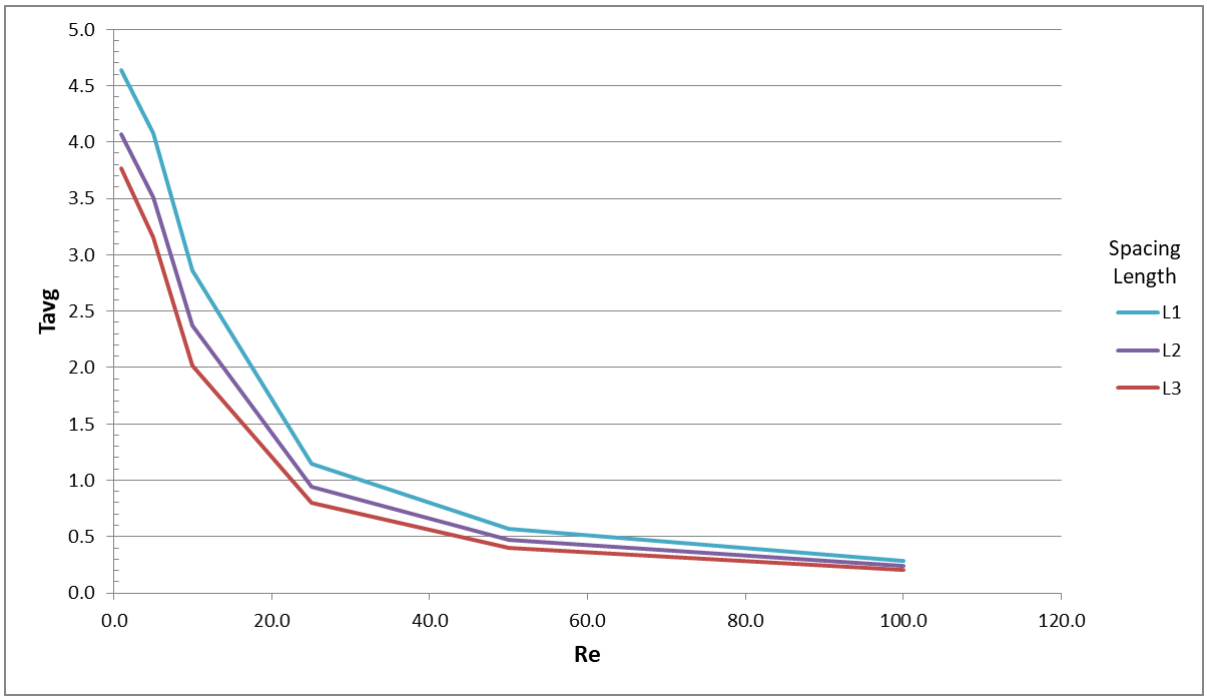

Figure 12. Temperature by Reynolds for different spacing lengths for the constant heat flux boundary condition. In this figure, L1, L2 and L3 are, respectively, 60, 120 and 180 units of lattice length of space between objects.

For the average temperature, the behavior is straightforward: the smaller spacings between objects produce a higher average temperature and the higher Reynolds numbers result in a smaller average temperature, which is exactly as expected.

5. CONCLUSION

This paper studied the heat transfer and flow of a channel with obstacles, varying spacing length between said obstacles. Two boundary conditions were simulated, constant heat flux and prescribed temperature. For each case, various values of Reynolds number were simulated.

The main conclusion is, as expected, that a greater number of obstacles (a smaller spacing between obstacles in a fixed length) results in an increase of friction but also an increase in heat exchange for all situations. However, the relation between Nusselt and Reynolds vary according to boundary condition and Reynolds range.

The Nusselt number dependency with Reynolds is quite different for each boundary condition. For the prescribed temperature boundary condition it was observed that an increase in the Reynolds number would result in a decrease of the Nusselt number for a small enough Reynolds number (Re from around 1 to 20). This behavior was reversed for higher Reynolds numbers. On the other hand, for the constant heat flux boundary condition, the increase of Nusselt with the increase of Reynolds number is remarkably greater for small Reynolds numbers (from around 1 to 10), while it stabilizes in a smaller rate of increase for Reynolds numbers greater than 10.

For the prescribed temperature boundary condition, for Reynolds between 1 to 20, Nusselt values start at around 3.1 for L2 and L3 (the two biggest spacing lengths between obstacles) and 3.3 for L1 (the smaller spacing length) and decrease with an increase of Reynolds to values around 2.8 for L2 and L3 and 3.0 for L1. For Reynolds from 20 to 100, Nusselt increases to around 2.9 for L2 and L3 and to around 3.2 for L1. It is to be expected that Nusselt numbers will surpass its value for Reynolds at 1 if Reynolds is to be increased further than 100.

For the constant heat boundary conditions, for Reynolds between 1 to 10, Nusselt values start at around 0.5 for all spacings and increase to around 2.75 for L2 and L3 and to around 3 for L1. For Reynolds from 10 to 100, Nusselt values increases to around 3 for L2 and L3 and to around 3.5 for L1.

The Darcy friction factor behaves the same for both boundary conditions, with a steep drop for lower Reynolds numbers. For Reynolds from around 1 to 10, L1 and L2 start at fD around 170 and L3 around 140, all of them dropping to around 20 at Reynolds around 10. For Reynolds greater than 10, all three spacing lengths seem to tend asymptotically to 0, having a value of around 4 for Reynolds around 20 and a value around 1 for Reynolds around 100.

6. REFERENCES

Borquist, E., Thapa, S. and Weiss, L., 2016. "Experimental and lattice Boltzmann simulated operation of a copper micro-channel heat exchanger". *Energy Conversion and Management*, Vol. 117, pp. 171–184. ISSN 01968904. doi: 10.1016/j.enconman.2016.02.066. URL http://dx.doi.org/10.1016/j.enconman.2016.02.066.

Ghadirzadeh, S. and Kalteh, M., 2017. "Lattice Boltzmann simulation of temperature jump effect on the nanofluid heat transfer in an annulus microchannel". *International Journal of Mechanical Sciences*, Vol. 133, No. May, pp. 524–534. ISSN 00207403. doi:10.1016/j.ijmecsci.2017.09.013. URL http://dx.doi.org/10.1016/j.ijmecsci.2017.09.013.

Jahanshaloo, L., Sidik, N.A.C., Fazeli, A. and Mahmoud, M.P., 2016. "An overview of boundary implementation in lattice Boltzmann method for computational heat and mass transfer". *International Communications in Heat and Mass Transfer*, Vol. 78, pp. 1–12. ISSN 07351933. doi:10.1016/j.icheatmasstransfer.2016.08.014. URL http://dx.doi.org/10.1016/j.icheatmasstransfer.2016.08.014.

Lou, Q., Guo, Z. and Shi, B., 2013. "Evaluation of outflow boundary conditions for two-phase lattice boltzmann equation". *Phys. Rev. E*, Vol. 87, p. 063301. doi:10.1103/PhysRevE.87.063301. URL https://link.aps.org/doi/10.1103/PhysRevE.87.063301.

Mesa, A.M., 2014. *Study of Lattice Boltzmann Boundary Conditions for Fluid Structure Interaction*. Master's thesis, Universidad EAFIT, Medellín.

Schlichting, H., 1979. *Boundary Layer Theory*. McGraw-Hill Book Company, 7th edition.

Zou, Q. and He, X., 1996. "On pressure and velocity flow boundary conditions and bounceback for the lattice Boltzmann BGK model". pp. 1–19. ISSN 1070-6631. doi:10.1063/1.869307. URL http://arxiv.org/abs/comp-gas/9611001%0Ahttp://dx.doi.org/10.1063/1.869307.

7. RESPONSIBILITY NOTICE

The author(s) is (are) solely responsible for the printed material included in this paper.